APL Photonics

Phase singularity annihilation in plasmonic nano-apertures via epsilon-near-zero metamaterials

Cite as: APL Photonics **6**, 016101 (2021); https://doi.org/10.1063/5.0031602
Submitted: 02 October 2020 . Accepted: 13 December 2020 . Published Online: 06 January 2021

F. Ghasemzadeh, A. R. Rashed, and H. Caglayan

Phase singularity annihilation in plasmonic nano-apertures via epsilon-near-zero metamaterials

Cite as: APL Photon. 6, 016101 (2021); doi: 10.1063/5.0031602
Submitted: 2 October 2020 • Accepted: 13 December 2020 •
Published Online: 6 January 2021

F. Ghasemzadeh, A. R. Rashed, and H. Caglayan[a]

AFFILIATIONS

Faculty of Engineering and Natural Sciences, Tampere University, 33720 Tampere, Finland

[a]Author to whom correspondence should be addressed: humeyra.caglayan@tuni.fi

ABSTRACT

In this work, we performed an extensive theoretical and experimental study to unveil the underlying mechanisms related to the intensified transmittance in epsilon-near-zero (ENZ)-integrated plasmonic nano-apertures. The occurrence of phase singularities at the incident side of plasmonic nano-apertures results in the reduction in transmittance. We show that transmittance enhancement in ENZ-integrated nano-slits is attributed to the annihilation of the phase singularities by the ENZ layer and subsequently the modification in plasmonic fields of metallic apertures. The singularity annihilation via ENZ metamaterials eliminates the abrupt changes in the phase of the Poynting vector underneath the slit, which results in a stronger cavity resonance inside the aperture. Due to this fact, a nano-aperture on top of an ENZ metamaterial is the only effective configuration to enhance the transmittance in ENZ-integrated nano-apertures. Hence, our study reveals the physics of the transmittance enhancement through ENZ-integrated plasmonic nano-apertures.

I. INTRODUCTION

With recent advances in optics, researchers reach the limits of the optical devices with conventional methods and materials. Exploiting structures with subwavelength features requires new designs and new materials. One of the tools to overcome this obstacle and beat the diffraction limit is to use epsilon-near-zero (ENZ) metamaterials.[1] ENZ metamaterials are defined as a group of optical materials in which the real part of their permittivity transients from the dielectric to metallic regime in one or several frequencies. These metamaterials have been known for over half a decade possessing different extraordinary optical properties.[2] As the permittivity of the material approaches toward zero, consequently, the wavelength becomes longer even at higher frequencies. This results in an extremely small value of wavenumber and subsequently an extremely high value of phase velocity.[3] Furthermore, such a relatively infinite value of phase velocity results in a static behavior of the propagating wave inside an ENZ medium and subsequently lifting the spatial constraints for phase conservation.[4,5] Additionally, the enhanced field inside the ENZ medium leads to a highly intense directional beam at the exit face of the medium.[6] ENZ-integrated metamaterials span a variety of applications such as chirality enhancement,[7] perfect absorption,[8] super-coupling,[9] phase engineering,[10] and super-lenses.[11]

Some natural materials such as gold and silver satisfy the requirement of an ENZ in the UV region. However, due to high optical losses, their performance as an ENZ structure is hindered. Besides, artificial ENZ structures with multilayer nanostructures[12,13] have been studied for the visible range. On the other hand, transparent conductive oxides (TCOs) such as indium tin oxide (ITO) and aluminum doped zinc oxide (AZO) are promising candidates to realize low-loss ENZ properties in the near and mid-infrared spectral regions. Prior studies show that the ENZ wavelength of these materials can be varied based on doping concentration and composition.[14,15]

Another phenomenon that has numerous applications in the manipulation of electromagnetic waves is surface plasmons, which are coherently oscillating free electrons that reside in the interface of the metal and dielectric. There are two categories of surface plasmons, namely, propagating surface plasmons (PSPs) and

localized surface plasmons (LSPs).[16] Recently, several works have shown that the combination of ENZ metamaterials with plasmonic nanostructures opens promising routes for ultimate control and enhancement of the light–matter interaction such as strong coupling between the plasmonic and ENZ mode,[17,18] drastic nonlinear enhancement,[19] controlling plasmonic modes in a nanoantenna array,[20] and modification of the spontaneous emission rate.[21]

One of the configurations for an ENZ-integrated plasmonic structure is a nano-slit placed over a thin ENZ layer. This can be utilized in molecular sensing,[22] enhanced spectroscopy,[23] and single-molecule trapping inside individual holes.[24] Some previous studies investigated analytically and experimentally different configurations of ENZ-integrated nano-apertures to enhance the transmittance efficiency of the device. Alu *et al.* theoretically analyzed a single subwavelength aperture in a perfectly electric conducting layer, which is covered by a low-k metamaterial in both entrance and exit faces. Their investigations show that the achieved transmission enhancement is sensitive to the optical losses of the applied materials and geometrical and electromagnetic parameters of the design.[25] Another study reported light funneling through an aperture that is placed on top of an ENZ layer and compares its functionality with two other cases that the ENZ material is filled in the aperture air gap and the ENZ filled aperture is placed between two ENZ layers.[26] Their analytical and experimental analyses reveal a correlation between transmission enhancement efficiency and the optical losses of the used ENZ material. Hajian *et al.* proposed a plasmonic aperture that is sandwiched between two ITO layers. The physical reasoning to explain the reported enhancement for the propagating TM-polarized light through a plasmonic slit is tied to the directionality and amplification of amplitude of light inside the ENZ medium.[27] However, none of these studies provide a clear illustration of the phase preservation inside and adjacent to the plasmonic slit. The assumption of a fully conserved phase in the entrance face of a plasmonic aperture is not fully true.

Phase singularities form in points that the intensity of the Poynting vector vanishes and therefore the optical phase becomes undetermined.[28,29] Prior studies showed that the existence of these points prevent the uniform flow of the energy at the incident side of the slit and subsequently inhibit the transmittance efficiency of subwavelength apertures.[30–32] Schouten *et al.*[32] analyzed the power flow near the plasmonic slit and showed the annihilation of singularity points by modifying waveguide modes via adjusting slit's parameters, which results in an enhancement in the total transmittance of a plasmonic slit. Therefore, modification in plasmonic fields of the metallic aperture in the presence of the ENZ metamaterial needs a deeper look into the subject to unleash the promising applications of ENZ-integrated nano-apertures.

With the present study, we show that the existence of phase singularities at the incident side of a plasmonic subwavelength slit is the main obstacle to intensify the transmitted light, as these singularity points suppress the intensity of the formed localized fields inside the cavity. To implement our investigation, we designed and fabricated structures with single and triple slits on an ITO thin film that acts as an ENZ metamaterial. The performed theoretical investigations strongly support the experimentally acquired transmittance enhancement. The observed strong funneling through ENZ-integrated nano-apertures is attributed to the annihilation of the formed phase singularities in the proximity of the metallic structure. This allows transmittance enhancement via the intensification of the localized plasmonic modes inside the aperture. We show that the most effective funneling enhancement strategy is to place a nano-aperture on top of an ENZ layer since the singularity points only form at the entrance face of a plasmonic aperture.

II. RESULTS AND DISCUSSION

In this study, two different structures including single and triple slits (three parallel single slits), placed over a 40 nm ITO film, are used. The fused silica (FS) is utilized as a transparent optical substrate for all of the structures. A 50 nm Gold (Au) film is considered as a plasmonic material with strong PSP properties in the near-infrared (NIR) spectral range.[33] The schematic in Fig. 1(a) shows the design for harnessing capabilities of ENZ metamaterials to achieve intensified transmittance in a plasmonic triple slit (three parallel single slits). The optical characteristics of the ITO thin film as an ENZ metamaterial in our structure are investigated. The complex permittivity is determined by a fit procedure based on the Drude model that predicts the transmittance and reflectance of the ITO layer. Figure 1(b) shows the real and imaginary parts of the permittivity of the ITO layer. Figure S1(a) depicts the experimentally acquired transmittance and reflectance of a 40 nm ITO film. The transition of the permittivity from the dielectric to metallic regime determines the ENZ region of the ITO layer around 1400 nm. For a low-loss material, the ENZ wavelength is specified when both the real and imaginary values of the dielectric constant become equal [see Fig. S1(b) of the supplementary material]. The enhancement factor for the designed structures is defined as the ratio of the transmission intensity in the presence and the absence of the ITO layer.

The enhancement factor vs slit width for a single slit, which is calculated based on the results presented in Figs. S2(a) and S2(b), is shown in Fig. 1(c). The maximum enhancement factor happens in the ENZ region (1300 nm–1500 nm) around 1425 nm, showing

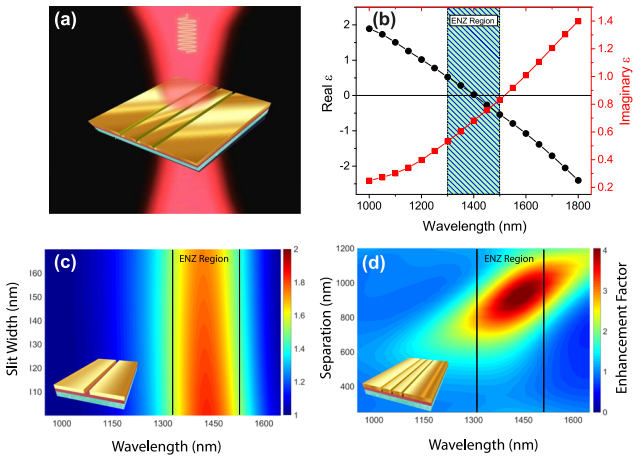

FIG. 1. (a) Schematic of the ENZ-integrated triple slit. (b) Corresponding real and imaginary parts of the permittivity for 40 nm ITO film. The calculated enhancement factor for (c) single nano-slit and (d) triple nano-slit. For both structures, an enhancement is observed in the ENZ region (1300 nm–1500 nm).

a higher transmittance after adding the ITO layer. One can spot the fact that the enhancement is maximum in the ENZ region for slit width less than 130 nm. However, due to low transmittance and fabrication restraints, a slit width of 140 nm is chosen in this study. For the triple-slit design, another main varying parameter is the separation between the nano-slits. Figure 1(d) demonstrates the enhancement factor of a triple slit as the separation between single slits is varied from 300 nm to 1200 nm. This enhancement factor is extracted based on the results presented in Figs. S2(c) and S2(d). The footprint of the ENZ material is easily visible in the performance of the device, as the maximum transmittance enhancement occurs in the ENZ region around 1450 nm for separation gaps in the vicinity of 950 nm. Changing the separation gap leads to a constructive or destructive superposition of generated PSPs, which results in suppression or enhancement of transmittance in a multi-slit design.[34] According to the presented results in Fig. 1(d), the separation gap of 950 nm shows the most efficient interference between multiple PSP modes, resulting in the highest enhancement factor for a triple-slit design.

While TM-polarization (the linear polarization state of the incident light is perpendicular to the long axis of the slits) simulations show enhancement, TE polarization (the orientation of the polarized light is parallel to the long axes of the slits) results show no enhancement [Figs. S3(a) and S3(b)]. Furthermore, due to the introduced loss by the ITO layer, the intensity of the transmitted light through both single and triple slits suppresses. This signifies that even if the introduced funneling by ITO may play a role in the transmittance enhancement process, but the optical loss of ITO conquers in this competition, and consequently, we end up with transmittance suppression. One needs to note that the introduced funneling by ITO is independent of the polarization state of the light. This means that the influence of this effect in the observed enhanced transmittance for TM-polarized light should be neglected as well.

The study of multiple nano-slits can help one to further understand the interaction between single apertures. Figure 2(a) shows the enhancement factor for a multi-slit with separation gaps of 950 nm. The data analysis provided in Sec. II of the supplementary material (Fig. S4) explains the linear growth of the multi-slit enhancement factor, as the number of the slits increases. Evidently, there is a direct relation between the number of slits and the enhancement factor. To identify the effect of multiple slits on the enhancement factor, one can divide this parameter by the number of slits [Fig. 2(b)]. The achieved per slit enhancement factor shows the contribution of each individual slit in the enhancement factor of a multi-slit design. It is evident that a triple slit exhibits the most efficient per slit enhancement factor compared to others. It is ferreted out that increasing the number of slits more than three has an unsatisfactory effect on the per slit enhancement factor. According to the presented results in Fig. 2, we have considered the study of the triple-slit design more intriguing compared to four or more numbers of slits.

The designed single and triple slits are fabricated by milling a 50 nm Au layer, which is coated on FS and FS/ITO substrates. Figures 3(a) and 3(b) show the SEM images of the fabricated single and triple slits, respectively. In addition, the cross-sectional view of the triple-slit design is presented in Fig. S5 to present the desired thicknesses of deposited Au and ITO layers and the precise milling of the Au layer with minimum damage on the ITO layer. Both control (without the ITO layer) and main (with the ITO layer) samples are characterized by the combination of a confocal microscope and a broadband NIR beam (see Sec. X in the supplementary material for more details). The transmittance of both sample groups is acquired with respect to a FS substrate. The results of the implemented measurements are presented in Figs. 3(c) and 3(d) for both TM and TE-polarized light. The comparison of the acquired results for TE and TM polarizations proves that the enhancement of the transmission only occurs for the incident beam with the TM polarization state, which is in agreement with the simulations, presented in Figs. S3(a) and S3(b). The transmittance enhancement is stronger for a triple slit compared to a single slit. An enhancement factor of 1.7 and 2.1 is extracted for an ENZ-integrated single slit and triple slit at the wavelength of 1480 nm, respectively. The corresponding enhancement factor of a simulated single slit is calculated as 1.7, while for a triple slit with a separation gap of 1 μm, this parameter is calculated as 3.2 [Figs. 1(c) and 1(d)]. There is good agreement between the calculated and experimentally acquired enhancement factors for both

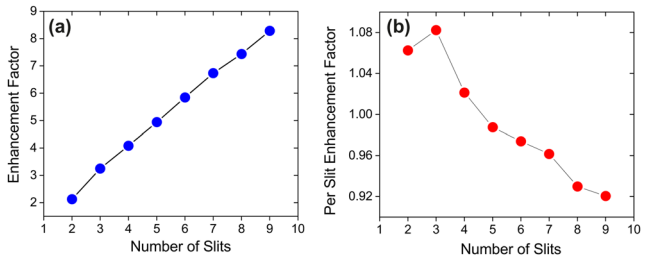

FIG. 2. (a) Calculated enhancement factor for a multi-slit from two to nine slits. (b) Per slit enhancement factor for the corresponding multi-slits of panel (a). The enhancement factor for each multi-slit is calculated at maximum enhanced transmittance wavelength as the ratio of the transmittance in the presence and absence of the ENZ layer.

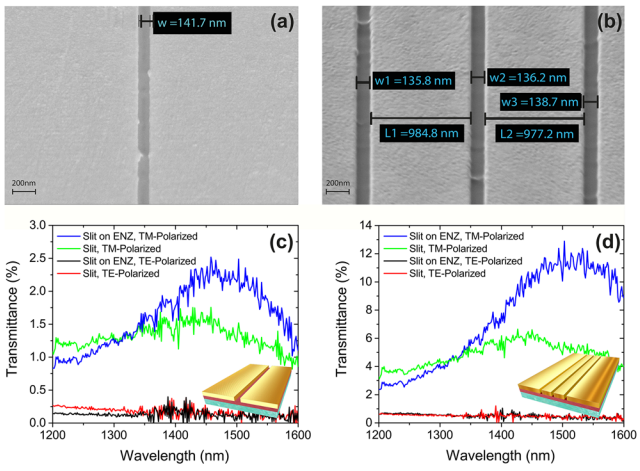

FIG. 3. SEM images of the fabricated samples for (a) a single slit and (b) a triple slit on the ITO layer. Transmittance of TM-polarized and TE-polarized light through (c) a single slit and (d) a triple slit in the presence and the absence of the ITO layer. The acquired experimental results prove that the transmittance enhancement occurs only for TM-polarized light.

single and triple slits. However, in the triple slit, due to the slight deviations in slit width and separation gaps in the fabrication process of each slit, there is a slight difference between the simulation and experimental results. This may explain the observed red-shift of enhanced transmittance for the triple-slit structure with respect to the calculated results. Another approach for extracting the enhancement factor can be defined based on the division of the transmitted signals in the peak wavelengths of the resonances. By considering such criteria, the calculated enhancement factors from the simulation results for a single slit and triple slit will be 1.7 and 2.8, while from the experimental results, it will be 1.5 and 1.9.

Figure 4(a) depicts the orientation and intensity of the time-averaged Poynting vectors for a single slit etched in a Au layer over a FS substrate. It is seen that at points A and B marked with red circles, there are spots of the Poynting vector with zero length. These points represent areas with zero intensity or magnitude for the Poynting vector in which the phase is infinitely undetermined. The power flow forms a half saddle in these two marked areas with a singularity in the phase of the propagating electromagnetic field. A close view of the wavefront around singularity point A is illustrated in the inset of Fig. 4(a). Those singularities prevent the smooth flow of energy near the slit and annihilation of them will increase the total transmittance of the slit. As presented in marked point A, the length of the Poynting vector is zero and power flow is moving in two opposite directions, forming a half of an electromagnetic field's Poynting vectors. The center of the represented phase and Poynting vectors fields is considered the point of singularity. The formation of the singularity points depends on the formation of LSPs and subsequently PSP modes, which appears only for the TM polarization state of the light. Furthermore, it is shown that any changes in the slit size can create or annihilate new phase singularities through modifying plasmonic fields.

Figure 4(b) represents the occasion when an ITO layer is introduced to the single slit structure. One can see that the ITO layer enhances the electric field inside the slit and at the same time eliminates these two observed phase singularities. Thus, the presence of the ENZ metamaterial cancels phase singularities and leads to a more uniform electromagnetic field, resulting in a higher transmittance through the slit.

Figures 4(c) and 4(d) show phase variations of the time-averaged Poynting vector, formed by TM-polarized incident light, for a single slit with a width of 140 nm in the absence and presence of the ITO film, respectively. The phase variation is extracted according to the real part and absolute value (magnitude) of the calculated complex Poynting vector (for details, see the supplementary material, Sec. VI). In panel (c), the disturbed phase variations near the rims of the slit result in the suppression of the transmitted light through the slit. However, adding the ENZ material beneath the slit preserves the phase on both sides of the slit, which diminishes the phase distributions. The observed phase conservation inside the ITO layer leads to an enhanced transmittance, despite the optical losses in ITO, which attenuates the light intensity. Figures S5(a) and S5(b) demonstrate phase variation for a triple-slit, before and after adding an ITO layer. A similar phase correction is observed for a triple slit compared to that of a single nano-slit. The phase gradient in panel (c) shows abrupt changes near the entrance of the slit in the range of 0 to pi, as the color changes from blue to yellow. Such a phase change that originates from the interaction of the incident light with the formed PSPs at the interface of the Au and FS surface correlates with the formed singularity points. On the other hand, the presence of the ENZ material reverses the Poynting vector direction in the left side of point A and the right side of point B [Fig. 4(b)], which results in a tailored wavefront [inset Fig. 4(b)]. The uniform gradient of the phase in the ITO layer [Fig. 4(d)] explains the parallel Poynting vectors underneath the slit [Fig. 4(b)]. Due to the ITO layer, the annihilation of the formed singularity point occurs, and a smooth wavefront forms under the nano-slit.

Figures S6(a) and S6(b) demonstrate phase variation for a triple slit in the absence and presence of the ITO layer. A similar phase correction is observed for a triple slit. Such a directive power flow

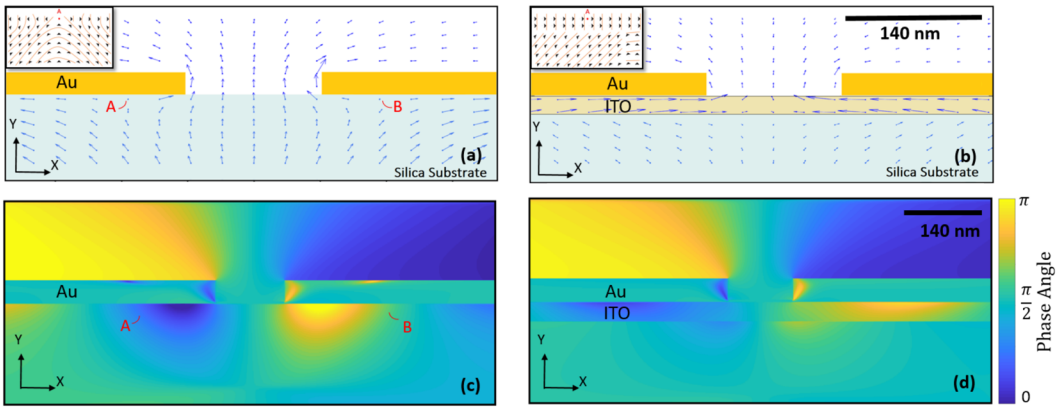

FIG. 4. Time-averaged Poynting vectors formed from a TM-polarized incident light at 1425 nm for a single slit with a width of 140 nm (a) in the absence and (b) in the presence of ITO. In panel (a), in marked points A and B, the length of the Poynting vector is zero, and power flow is moving in two opposite directions. In panel (b), due to the presence of the ENZ layer, the singularities in points A and B are eliminated. The applied two different normalizations for Poynting vectors in panels (a) and (b) result in the size difference of the vectors. Phase variations of the time-averaged Poynting vectors for the same slit (c) in the absence and (d) in the presence of ITO. Insets of panels (a) and (b) illustrate the close view of the wave-front around singularity point A without and with the ITO layer, respectively.

toward the entrance of the slit interacts constructively with cavity resonances of the slit, which leads to a stronger light funneling through the slit with the pi/2 phase. This fact is depicted in Fig. S7, which compares the magnitude of the Poynting vectors in the presence and absence of the ITO layer. The funneling is evident in the cavity area, which shows an efficient out-coupling of the energy through the slit after adding the ENZ layer.

Figures 5(a) and 5(b) show the distribution of the x-component of the electric field. The enhanced field inside the aperture indicates the presence of the LSP mode (cavity mode) in the air gap of the designed slit. It is worthy to note that only for TM-polarization of the incident light, the surface charges can be induced on the walls of the slit. These induced charges are in opposite phases at two sides of the slit.[35,36] Consequently, an electric field spanning from a positive to a negative charge is formed, resulting in an efficient out-coupling of the transmitted light through the slit.[37] Figure 5(b) shows a stronger LSP mode between the walls of the nano-slit when it is placed on top of the ENZ metamaterial. It is evident in Fig. S7 that the magnitude of the Poynting vector is enhanced when the ITO is introduced under the slit. The annihilation of the phase singularities in the presence of the ITO enhances the transmission and intensifies the electromagnetic field through the slit. Thus, the existence of the ENZ metamaterial beneath a nano-slit leads to the formation of a stronger LSP mode in the air gaps of the metallic slit. Our study shows the correlation between the enhancement factor and the strength of the LSP modes inside the nano-aperture, in which stronger LSP modes result in a higher transmittance. In fact, the localized fields in nano-slit walls operate as nanoantennas to out-couple efficiently the near field to the far-field.[38] The mentioned effect operates as the main channel to create better funnelling through the nano-aperture. Therefore, due to the lack of LSP modes for TE polarization of the light in the air gap of the aperture, the transmittance enhancement after adding the ITO layer is not observed (Fig. S3).

The y-component of the electric field reveals the formation of PSP modes. Near the rims of the slit, the PSP modes are in the opposite phases on both sides of the Au film. It should be taken into account that due to the difference in the surrounding dielectric medium for the upper and lower interfaces of the Au film, the wavelength of the generated PSPs is different.[16] By changing the study wavelength, one can observe that the formed PSPs appear at different phases.[39] The comparison of PSP modes in panels (c) and (d) of Fig. 5 shows that the presence of the ENZ material enhances the PSPs at the interface of the metal and ITO layers. This occurs due to the strong field confinement inside the ITO, resulting from the imposed boundary conditions at the interface of the Au and the ENZ layer.[40] One can see that by adding the ENZ layer, the intensity of the PSP modes enhances at the slit–air interface as well. This may explain the correlation between the intensity of the LSP and PSP modes, in which stronger LSPs result in more intensified PSP modes.

Due to similarity of the x-component of the electric field for single and triple slits, the $\vec{E}_x$ field profiles of the triple slit is not shown. Figure 6 compares the calculated y-component of the electric field ($\vec{E}_y$) for a triple slit in the presence and the absence of a 40 nm ITO layer. In Fig. 6(b), the enhancement of fields inside the ENZ layer and symmetrically formed PSPs in the surfaces of the Au film are apparent. A comparison of the triple slit's electric fields in Figs. 6(a) and 6(b) with corresponding single slit's electric fields in Figs. 5(a) and 5(b) shows the consistency in the phase of PSP modes formed around the rims of each slit. One can achieve the maximum possible transmittance for the triple-slit design in which for particular separation gaps, the constructive interference between PSPs can take place [Fig. 1(d)]. The confinement of E_y in the ITO layer is evident in Fig. 6(b). This phenomenon is observed for an ENZ-integrated single slit, as well. However, in the triple-slit design, due to the interaction between generated PSPs of adjacent slits, the part of the ENZ layer under the central slit shows a slightly stronger field than the corresponding field in other slits.

Former studies show that adding an ENZ metamaterial on top of a subwavelentgh slit[25,27] or embedding it inside the slit air gap[26] does not help to improve the enhancement factor. Paradoxically, due to the introduced losses by the added ENZ metamaterial as well as degradation of the LSP and PSP fields (Fig. S8), the enhancement factor of the ENZ-integrated slit suppresses. The phase variations do not form singularity points at the exit side or inside the plasmonic

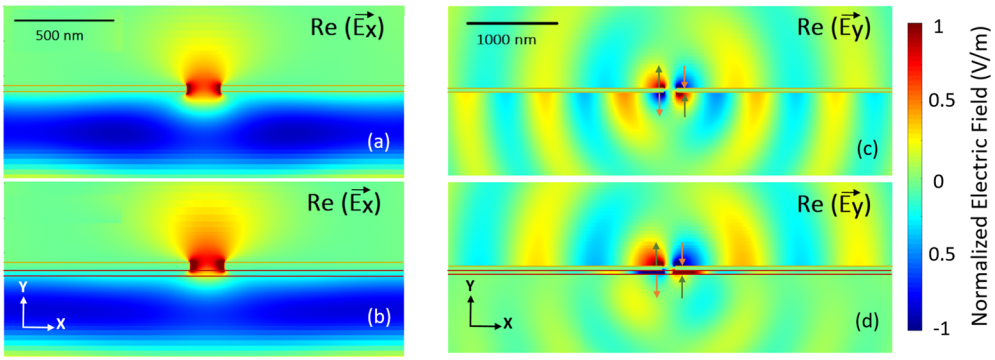

FIG. 5. The x-component of the E-field at λ = 1425 nm for a 140 nm slit milled in a 50 nm Au film (a) on a FS substrate and (b) on the ITO layer deposited on a FS substrate. The y-component of the E-field of the same structure (c) on a FS substrate and (d) on the ITO layer deposited on the FS substrate. The arrows show the direction of the strongest electric fields (e.g., Ex, Ey). The dark red color indicates upward electric field vectors (+y), while the dark blue color indicates downward vectors (−y).

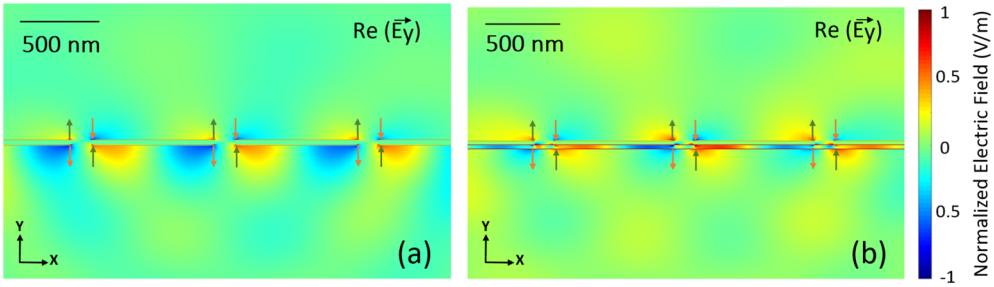

FIG. 6. Distributions of the E_y field for triple slits (a) without ITO and (b) with the ITO layer. The modification in the E_y field distribution around the rims of the slits is visible by adding the ITO layer.

apertures but at the entrance side. Therefore, the only effective configuration to improve the enhancement factor is to add an ENZ metamaterial beneath the aperture.

III. CONCLUSION

In this work, an inclusive study of transmittance enhancement in ENZ-integrated plasmonic nano-slits is performed. The enhancement factors of the designed single and triple slits are calculated and measured in the ENZ region of a thin ITO layer. We established the ENZ-mediated enhancement by employing phase tailoring and subsequently the intensification of cavity mode in the presence of the ENZ metamaterial. The experimental measurements and theoretical analyses on the electric field, Poynting vector, and phase profiles of the nano-slits reveal the mechanisms behind the observed intensified transmittance. We showed that according to the formation of the phase singularities at the incident side of the nano-aperture, the only effective ENZ-integrated configuration that can enhance the transmittance is an aperture that is placed on top of an ENZ layer. Such configuration increases the enhancement factor through annihilation of the singularity points and uniforms the electric field phase underneath the nano-slit. We believe that these results open a new avenue toward a deeper understanding of the underlying physics related to the light funneling through ENZ-integrated plasmonic nano-apertures. Moreover, the inhibition of the singularity points by an ENZ metamaterial might offer interesting technological possibilities, e.g., in the tailoring of optical forces in integrated devices.

SUPPLEMENTARY MATERIAL

See the supplementary material for optical characteristics of the ITO layer, simulated transmittance results, cross-sectional SEM image of the triple slit, Poynting vector calculations, electric field profiles for different ENZ-integrated nano-slits, and methods for simulation, fabrication, and characterization.

AUTHORS' CONTRIBUTIONS

F.G. and A.R.R. contributed equally to this work.

ACKNOWLEDGMENTS

The authors would like to thank Mohsin Habib for his help in collecting the cross-sectional images of the samples. We acknowledge the financial support of Academy of the Finland Flagship Programme (PREIN) (Grant No. 320165).

DATA AVAILABILITY

The data that support the findings of this study are available from the corresponding author upon reasonable request.

REFERENCES

[1]Z. J. Wong, Y. Wang, K. O'Brien, J. Rho, X. Yin, S. Zhang, N. Fang, T.-J. Yen, and X. Zhang, "Optical and acoustic metamaterials: Superlens, negative refractive index and invisibility cloak," J. Opt. **19**, 084007 (2017).
[2]M. G. Silveirinha and N. Engheta, "Theory of supercoupling, squeezing wave energy, and field confinement in narrow channels and tight bends using ε near-zero metamaterials," Phys. Rev. B **76**, 245109 (2007).
[3]M. H. Javani and M. I. Stockman, "Real and imaginary properties of epsilon-near-zero materials," Phys. Rev. Lett. **117**, 107404 (2016).
[4]N. Engheta, "Pursuing near-zero response," Science **340**, 286–287 (2013).
[5]Y. Li and N. Engheta, "Supercoupling of surface waves with ε-near-zero metastructures," Phys. Rev. B **90**, 201107 (2014).
[6]A. Alù, N. Engheta, A. Erentok, and R. W. Ziolkowski, "Single-negative, double-negative, and low-index metamaterials and their electromagnetic applications," IEEE Antennas Propag. Mag. **49**, 23–36 (2007).
[7]C. Rizza, X. Li, A. Di Falco, A. Marini, E. Palange, and A. Ciattoni, "Diode-like asymmetric transmission in ultrathin hyperbolic epsilon-near-zero slabs: Extreme anisotropy mimicking chirality," arXiv:1802.07017 (2018).
[8]S. Feng and K. Halterman, "Coherent perfect absorption in epsilon-near-zero metamaterials," Phys. Rev. B **86**, 165103 (2012).
[9]B. Edwards, A. Alù, M. E. Young, M. Silveirinha, and N. Engheta, "Experimental verification of epsilon-near-zero metamaterial coupling and energy squeezing using a microwave waveguide," Phys. Rev. Lett. **100**, 033903 (2008).
[10]A. Alu, M. G. Silveirinha, A. Salandrino, and N. Engheta, "Epsilon-near-zero metamaterials and electromagnetic sources: Tailoring the radiation phase pattern," Phys. Rev. B **75**, 155410 (2007).
[11]V. Torres, B. Orazbayev, V. Pacheco-Peña, J. Teniente, M. Beruete, M. Navarro-Cía, M. S. Ayza, and N. Engheta, "Experimental demonstration of a millimeter-wave metallic ENZ lens based on the energy squeezing principle," IEEE Trans. Antennas Propag. **63**, 231–239 (2014).
[12]J. Gao, L. Sun, H. Deng, C. J. Mathai, S. Gangopadhyay, and X. Yang, "Experimental realization of epsilon-near-zero metamaterial slabs with metal-dielectric multilayers," Appl. Phys. Lett. **103**, 051111 (2013).

[13]A. R. Rashed, B. C. Yildiz, S. R. Ayyagari, and H. Caglayan, "Hot electron dynamics in ultrafast multilayer epsilon-near-zero metamaterials," Phys. Rev. B **101**, 165301 (2020).
[14]G. V. Naik, V. M. Shalaev, and A. Boltasseva, "Alternative plasmonic materials: Beyond gold and silver," Adv. Mater. **25**, 3264–3294 (2013).
[15]N. Kinsey, C. DeVault, J. Kim, M. Ferrera, V. M. Shalaev, and A. Boltasseva, "Epsilon-near-zero al-doped ZNO for ultrafast switching at telecom wavelengths," Optica **2**, 616–622 (2015).
[16]S. A. Maier, *Plasmonics: Fundamentals and Applications* (Springer Science & Business Media, 2007).
[17]V. Bruno, C. DeVault, S. Vezzoli, Z. Kudyshev, T. Huq, S. Mignuzzi, A. Jacassi, S. Saha, Y. Shah, S. Maier *et al.*, "Negative refraction in time-varying strongly coupled plasmonic-antenna—Epsilon-near-zero systems," Phys. Rev. Lett. **124**, 043902 (2020).
[18]B. C. Yildiz and H. Caglayan, "Epsilon-near-zero media coupled with localized surface plasmon modes," Phys. Rev. B **102**, 165303 (2020).
[19]M. Z. Alam, S. A. Schulz, J. Upham, I. De Leon, and R. W. Boyd, "Large optical nonlinearity of nanoantennas coupled to an epsilon-near-zero material," Nat. Photonics **12**, 79–83 (2018).
[20]M. Habib, D. Briukhanova, N. Das, B. C. Yildiz, and H. Caglayan, "Controlling the plasmon resonance via epsilon-near-zero multilayer metamaterials," Nanophotonics **9**, 3637–3644 (2020).
[21]V. Caligiuri, M. Palei, M. Imran, L. Manna, and R. Krahne, "Planar double-epsilon-near-zero cavities for spontaneous emission and purcell effect enhancement," ACS Photonics **5**, 2287–2294 (2018).
[22]A. B. Dahlin, "Sensing applications based on plasmonic nanopores: The hole story," Analyst **140**, 4748–4759 (2015).
[23]J.-F. Masson, M.-P. Murray-Méthot, and L. S. Live, "Nanohole arrays in chemical analysis: Manufacturing methods and applications," Analyst **135**, 1483–1489 (2010).
[24]A. A. Al Balushi, A. Kotnala, S. Wheaton, R. M. Gelfand, Y. Rajashekara, and R. Gordon, "Label-free free-solution nanoaperture optical tweezers for single molecule protein studies," Analyst **140**, 4760–4778 (2015).
[25]A. Alù, F. Bilotti, N. Engheta, and L. Vegni, "Metamaterial covers over a small aperture," IEEE Trans. Antennas Propag. **54**, 1632–1643 (2006).
[26]D. Adams, S. Inampudi, T. Ribaudo, D. Slocum, S. Vangala, N. Kuhta, W. Goodhue, V. A. Podolskiy, and D. Wasserman, "Funneling light through a subwavelength aperture with epsilon-near-zero materials," Phys. Rev. Lett. **107**, 133901 (2011).
[27]H. Hajian, E. Ozbay, and H. Caglayan, "Beaming and enhanced transmission through a subwavelength aperture via epsilon-near-zero media," Sci. Rep. **7**, 4741 (2017).
[28]J. Tong, A. Mercedes, G. Chen, and S. Boriskina, "Local field topology behind light localization and metamaterial topological transitions," in *Singular and Chiral Nanoplasmonics* (Pan Stanford Publishing, Singapore, 2014), pp. 259–284.
[29]D. V. Novitsky and A. V. Novitsky, "Optical poynting singularities of propagating and evanescent vector bessel beams," arXiv:0911.3754 (2009).
[30]H. F. Schouten, T. D. Visser, G. Gbur, D. Lenstra, and H. Blok, "Creation and annihilation of phase singularities near a sub-wavelength slit," Opt. Express **11**, 371–380 (2003).
[31]H. F. Schouten, T. D. Visser, G. Gbur, D. Lenstra, and H. Blok, "The diffraction of light by narrow slits in plates of different materials," J. Opt. A **6**, S277 (2004).
[32]H. F. Schouten, T. D. Visser, D. Lenstra, and H. Blok, "Light transmission through a subwavelength slit: Waveguiding and optical vortices," Phys. Rev. E **67**, 036608 (2003).
[33]P. R. West, S. Ishii, G. V. Naik, N. K. Emani, V. M. Shalaev, and A. Boltasseva, "Searching for better plasmonic materials," Laser Photonics Rev. **4**, 795–808 (2010).
[34]H. Schouten, N. Kuzmin, G. Dubois, T. Visser, G. Gbur, P. Alkemade, H. Blok, D. Lenstra, E. Eliel *et al.*, "Plasmon-assisted two-slit transmission: Young's experiment revisited," Phys. Rev. Lett. **94**, 053901 (2005).
[35]X. Huang, R. Peng, Z. Wang, F. Gao, and S. Jiang, "Charge-oscillation-induced light transmission through subwavelength slits and holes," Phys. Rev. A **76**, 035802 (2007).
[36]Y. Xie, A. R. Zakharian, J. V. Moloney, and M. Mansuripur, "Transmission of light through slit apertures in metallic films," Opt. Express **12**, 6106–6121 (2004).
[37]J. Olkkonen, *Finite Difference Time Domain Studies on Sub-Wavelength Aperture Structures* (VTT, 2010).
[38]V. Rivera, F. Ferri, O. Silva, F. Sobreira, and E. Marega, Jr., *Light Transmission via Subwavelength Apertures in Metallic Thin Films* (Intech, 2012).
[39]S.-H. Chang, S. K. Gray, and G. C. Schatz, "Surface plasmon generation and light transmission by isolated nanoholes and arrays of nanoholes in thin metal films," Opt. Express **13**, 3150–3165 (2005).
[40]V. T. Landivar, "Plasmonics and metamaterials at terahertz frequencies," Ph.D. thesis, Citeseer, 2014.